

Bi-layer Kinetic Inductance Detectors for space observations between 80-120 GHz

A. Catalano¹, J. Goupy², H. le Sueur³, A. Benoit², O. Bourrion¹, M. Calvo², L. Dumoulin³, F. Levy-Bertrand²,
J. Macías-Pérez¹, S. Marnieros³, N. Ponthieu⁴, and A. Monfardini²

¹ Laboratoire de Physique Subatomique et de Cosmologie, CNRS/IN2P3, Université Joseph Fourier Grenoble I, Institut National Polytechnique de Grenoble, 53 rue des Martyrs, 38026 Grenoble Cedex, France

² Institut Néel F-38042, CNRS, Université Joseph Fourier Grenoble I F-38042, 25 rue des Martyrs, Grenoble, France

³ Centre de Sciences Nucléaires et de Sciences de la Matière (CSNSM), CNRS/IN2P3, bat 104 - 108, 91405 Orsay Campus, France

⁴ Institut de Planétologie et d'Astrophysique de Grenoble (IPAG), CNRS and Université de Grenoble, France

Preprint online version: October 15, 2018

ABSTRACT

We have developed Lumped Element Kinetic Inductance Detectors (LEKID) sensitive in the frequency band from 80 to 120 GHz. In this work, we take advantage of the so-called proximity effect to reduce the superconducting gap of Aluminium, otherwise strongly suppressing the LEKID response for frequencies smaller than 100 GHz. We have designed, produced and optically tested various fully multiplexed arrays based on multi-layers combinations of Aluminium (Al) and Titanium (Ti). Their sensitivities have been measured using a dedicated closed-circle 100 mK dilution cryostat and a sky simulator allowing to reproduce realistic observation conditions. The spectral response has been characterised with a Martin-Puplett interferometer up to THz frequencies, and with a resolution of 3 GHz. We demonstrate that Ti-Al LEKID can reach an optical sensitivity of about $1.4 \cdot 10^{-17} \text{ W/Hz}^{0.5}$ (best pixel), or $2.2 \cdot 10^{-17} \text{ W/Hz}^{0.5}$ when averaged over the whole array. The optical background was set to roughly 0.4 pW per pixel, typical for future space observatories in this particular band. The performance is close to a sensitivity of twice the CMB photon noise limit at 100 GHz which drove the design of the Planck HFI instrument. This figure remains the baseline for the next generation of millimetre-wave space satellites.

Key words. instrumentation: detectors – space vehicles: instruments – methods: data analysis – cosmic background radiation

1. Introduction

The study of the Cosmic Microwave Background (CMB) temperature and polarisation anisotropies has become a powerful tool for cosmology thanks in particular to the spatial observations of the COBE (Kogut et al. 1996), the WMAP (Bennett et al. 2013) and Planck satellites (Planck Collaboration (2013 results I) 2014). The Planck mission has provided detailed temperature and polarisation CMB maps (Planck Collaboration et al. 2014), but it was not conceived as the ultimate instrument for CMB polarisation measurements and it will most probably only marginally measure primordial CMB polarisation B-modes. The latter are only sourced by tensor perturbations in the early universe and are predicted by inflation (Hu & White 1997). To improve this situation, new CMB space missions such as CORE+¹, PIXIE (Kogut et al. 2011), LiteBIRD (Matsumura et al. 2014), are under study.

In this context, space observations at about and slightly below 100 GHz have proved to be fundamental for CMB science, as they lie in the frequency range for which Galactic foreground contamination is minimal both in intensity and polarisation (Planck Collaboration et al. 2014; Fauvet et al. 2012, 2011). The Planck mission² was equipped with 11 HEMT (Low Frequency Instrument Mennella et al. (2011)) and 52 high

impedance bolometers (High Frequency Instrument Planck HFI Core Team et al. (2011)) observing from 30 GHz to 1 THz. Among those, 8 Polarised Sensitive Bolometers (PSB) with a bandpass centred at 100 GHz ($\Delta\nu/\nu = 0.33$) were used to survey the sky in temperature and polarisation at an angular resolution of about 10 arcmin. This provided HFI with a powerful tool to detect and precisely measure the CMB E-modes but not the primordial B-modes which are expected to be much fainter (Planck Collaboration et al. 2014). To meet the challenge of measuring CMB polarisation B-modes, it is necessary to improve the instrumental sensitivity by at least one order of magnitude with respect to Planck. In terms of Noise Equivalent Power this corresponds going from $10^{-17} \text{ WHz}^{-1/2}$ to $10^{-18} \text{ WHz}^{-1/2}$. This can be achieved by increasing the focal plane coverage, using thousands of Background Limited Instrument Performance (BLIP) contiguous pixels.

Kinetic Inductance Detectors (KID) (Day et al. 2003) have now reached a maturity adequate for space instruments. The first demonstration of this maturity was achieved by ground-based experiments and in particular by the New IRAM KID Array (NIKA) instrument. NIKA is a dual-band camera operating with frequency-multiplexed arrays of Lumped Element Kinetic Inductance Detectors (LEKIDs) based on Aluminium films and cooled at 100 mK (Monfardini et al. 2011). The NIKA instrument exhibits state-of-the-art sensitivity in the 120-300 GHz band range (Catalano et al. 2014).

The frequency range below 120 GHz is not accessible using the NIKA Aluminium films due to the superconducting gap cut-off. Therefore we need to adopt lower superconducting gap

Send offprint requests to: A. Catalano - catalano@lpsc.in2p3.fr

¹ http://www.core-mission.org/documents/CoreProposal_Final.pdf

² <http://www.esa.int/Planck>

films. Several authors have investigated Titanium Nitride (TiN) as an alternative to Aluminium KID (Swenson et al. 2013; Leduc et al. 2010; Bueno et al. 2014) in the last years. In parallel we have studied a large number of possible alternative solutions. Among them, we have investigated Nb(x)Si(1-x) as a promising alloy to be used at these frequencies (Calvo et al. 2014). Here we use a different approach: we start from Aluminium which has given the best performances up to now, and lower its gap using the superconducting proximity effect with Titanium.

This paper is structured as follows. In Sec. 2, we give the main ingredients of the bi-layer LEKID design and describe its fabrication process; details on the noise and responsivity of a LEKID array are also presented. In Sec. 3, we describe the experimental setup. Sec. 4 presents the measurements and the results obtained. We draw conclusions in Sect. 5.

2. LEKID Detectors

Here we review the basic ingredients necessary to discuss the design and to evaluate the performances of the Ti-Al bilayer LEKID. General KID theory was first established by Day et al. (2003). For a complete review, we suggest Zmuidzinas (2012) and Doyle (2008). LEKID is a resonator fabricated from superconducting elements in which absorbed photons can change the Cooper pair density producing a change in both resonant frequency and the quality factor of the resonator. LEKID arrays are based on series of LC resonators of different eigenfrequencies, coupled to a single 50 Ω feed-line. The term *Lumped Element* describes the fact that the resonator is small compared to the wavelength at the resonance frequency. In addition, Lumped Element devices act directly as the absorber of GHz - THz photons, which greatly simplifies the design and array fabrication. Furthermore, one needs to match their sheet impedance to the incoming photons, which implies using either very thin, or quite resistive layers. In that respect, Ti is preferable to noble metals such as Au, Ag or Cu for tuning the superconducting gap of Aluminium.

2.1. Tuning the gap cut-off with proximity effect

The minimum photon energy that can be absorbed in a superconductor below the critical temperature is equal to twice the superconducting gap Δ_0 . For standard³ superconductors:

$$\Delta_0 \approx 1.764 \cdot k_B T_c \quad (1)$$

where k_B is the Boltzmann constant and T_c is the critical temperature of the transition to the superconducting state.

Adjusting T_c is therefore important in order to tune the absorption of photons to the suitable frequency. The possibility of tuning the transition temperature of a superconductor through the proximity effect with a normal metal (or another superconductor) is a well-known property of superconductivity. It has been successfully exploited in transition edge sensors to operate bolometers at a lower temperature and hence lower their specific heat (Irwin & Hilton 2005). Here we also exploit the proximity effect, but in this case to lower the energy threshold of detectable photons.

A comprehensive calculation of the T_c of bi-layers is given in Martinis et al. (2000). More generally, all relevant properties (in

³ In this paper we name *standard superconductors* those that follows the superconductivity theory proposed by John Bardeen, Leon Cooper, and John Robert Schrieffer (BCS)

particular the density of states) can be derived in the framework of the Usadel theory (Usadel 1970), which describes inhomogeneous superconductors. One needs to solve (most often numerically) two coupled non-linear differential equations describing the diffusion of electronic excitations (single and paired) in an inhomogeneous pair potential, provided boundary conditions at the interfaces. Here we consider that the contact between the two layers is perfect and that the average transmission is unity, which provides the strongest proximity effect. Furthermore, the superconducting coherence length is assumed to be larger than the thickness of the film, and thereby superconducting properties are homogeneous over the thickness.

In that case, an approximate analytical solution can be derived following Cooper's intuitive approach (Cooper 1961), considering the bilayer as a superconductor with an effective pairing potential NV_{eff} . As electrons spend a fraction of time $N_1 d_1 / (N_1 d_1 + N_2 d_2)$ in layer 1, this effective potential writes:

$$NV_{eff} = \frac{N_1 V_1 (N_1 d_1) + N_2 V_2 (N_2 d_2)}{N_1 d_1 + N_2 d_2},$$

where N_x is the electron density, V_x the electron phonon coupling and d_x the thickness of layer x . This effective potential is then used to calculate T_c in the standard superconductors gap equation $k_B T_c \approx 1.13 \hbar \omega_D \cdot e^{(-1/NV_{eff})}$, where ω_D is the Debye frequency. This approach is valid only when the vibration properties of the two layers are identical, which is roughly the case for Ti and Al. From this simple formula, the general trend of which is confirmed by more thorough calculations, one notices the great convenience of bi-layers since their critical temperature can be finely tuned by changing the relative thickness of the components. For the Ti 10 nm/Al 25 nm bi-layers fabricated in this work, the expected T_c is between 850 mK and 920 mK. This uncertainty comes from the fact that we need to take into account an increase of the T_c of Al at 25 nm compared to the bulk value (the discussion of which is not the purpose of the present work). In a standard superconductor, this yields a frequency threshold for photon absorption between 62 GHz and 68 GHz. A last argument for choosing Ti rather than noble metals comes from its weak solubility in Al, which improves predictability, reproducibility and robustness of the devices to aging.

2.2. Optical Responsivity

The optical responsivity for a LEKID represents the relation between a variation of the incident optical power and the shift in the resonant frequency of the detector ($\mathfrak{R} = \frac{df}{dW}$). This measured variation is determined by the change in internal inductance of the film with a change in Cooper pair density induced by incoming photons.

For the LEKID, all the properties directly related to the calculation of the responsivity affect each other so that it is not possible to derive a general single analytical formula. For a detailed study of the parameters that determine the responsivity of a LEKID we refer to Doyle et al. (2007) and Doyle et al. (2008).

2.3. Noise

The detector Noise Equivalent Power (NEP), in W/\sqrt{Hz} , is defined as the optical signal that is equal to the noise in a 1 Hz amplifier bandwidth at the output. This quantity takes into account the response and the spectral noise density $S_n(f)$ of the

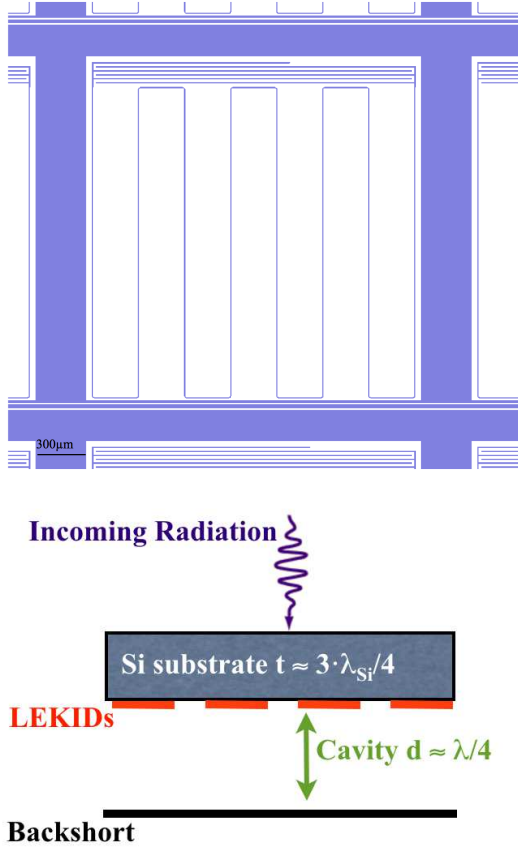


Fig. 1. Single Ti-Al bilayer LEKID resonator design (top). The resonator is composed of a long inductive meander line and a capacitive element used also for tuning the resonant frequency. The effective sheet impedance of the meander line (seen by GHz-THz photons) is adjusted by the geometrical filling factor, for a given the film resistivity. In order to optimise 100 GHz photon absorption, the pixels are back-illuminated through the Silicon substrate. In addition we use a back-short cavity situated at an optimised distance of $750 \mu\text{m}$ from the pixels (bottom).

detector (in $H\text{z}/\sqrt{H\text{z}}$). All the uncorrelated sources of noise add quadratically:

$$NEP_{tot}^2 = \sum_{i=1}^N NEP_{det(i)}^2 + \sum_{i=1}^N NEP_{el(i)}^2 + NEP_{phot}^2 \quad (2)$$

The detectors noise NEP_{det} may come from random variations of the effective dielectric constant or fluctuations of the Cooper pair density due to generation-recombination noise⁴. NEP_{el} is the noise associated to the full readout electronics chain (cold and warm). Finally NEP_{phot} represents the source of noise related to the photon noise which comes from the fluctuations of the incident radiation due to the Bose-Einstein distribution of the photon emission. This noise corresponds to the ultimate limitation in sensitivity of any instrument as it does not depend on detector performance and readout electronics. Considering a satellite orbiting around the second Lagrange point of the Earth-Sun system, the in-space photon noise level per pixel at 100 GHz is equal to about $0.5 \cdot 10^{-17} \text{ W}/\sqrt{H\text{z}}$.

⁴ In the case of NIKA Aluminum LEKID, the contribution of the detector noise has been measured to be lower than the other sources of noise and relatively flat in frequency

As a guideline, for future generation millimetre satellite as well as for Planck HFI, the goal NEP per pixel has been defined:

$$NEP_{GOAL} \leq 2 \cdot NEP_{phot} \quad (3)$$

When this condition is satisfied we refer to photon noise dominated detectors. We keep this definition as a reference to compare the results obtained in this paper.

2.4. LEKID module design, fabrication and assembly

For the first generation Ti-Al arrays, we adopted single polarisation LEKID designed originally for Aluminium films (Fig. 1). The first prototype of Ti-Al arrays comprises 25 pixels. The LEKID holder allows back-illumination through the Silicon substrate. This method works better than directly illuminating the LEKID as high permittivity silicon substrate has a far lower impedance than that of free space. In front of the LEKID, a superconducting lid acts as a $\lambda/4$ back-short, optimising the absorption in the frequency band of interest. A schematic of this arrangement is shown in Fig. 1

Each pixel is a resonator composed by a meander inductor and an interdigitated capacitor. The $4 \mu\text{m}$ wide lines of the meander are the smallest features in the current design. The 25 pixels are inductively coupled to a coplanar wave guide (CPW) 50Ω line. The fabrication starts with a high resistivity ($> 6000 \Omega \cdot \text{cm}$), $525 \mu\text{m}$ thick silicon [111] mono-crystalline wafer. The native silicon oxide is etched with an $\text{HF:H}_2\text{O}$ 5% solution, then rinsed in H_2O . This step passivates the Si bonds on the surface, replacing O with H. The wafer is then put under vacuum within the next 30 minutes, to prevent re-oxidation. The bilayer is coated *in situ* by e-beam evaporation under a $\approx 3e - 8 \text{ mb}$ vacuum. A 10 nm thick titanium film is first deposited, followed directly by a 25 nm thick aluminium film. This ensures that there is no oxidation layer at the interface between titanium and aluminium, and grants us a maximal proximity effect between the two layers. The next step is a standard photo-lithographic process, with a positive resin (AZ1512Hs). The etching is made in two phases, first with an Al-etch dip then a dilute 0.1 % HF solution to etch Ti. After dicing, the array is mounted in a dedicated holder, and the CPW is wire-bonded to the launcher with an Al-Si wire.

2.5. Readout system

We used a Vector Network Analyzer (VNA) to measure the LEKID responsivity and the NIKEL electronics (described in Bourrion et al. (2012)) to measure the spectral response and characterise the noise. The NIKEL electronics has been successfully used during several NIKA observing campaigns (Catalano et al. 2014; Adam et al. 2014). We briefly describe the readout concept: we generate a frequency comb which is up converted by mixing with a local oscillator carrier at the appropriate frequency, corresponding to the best estimate resonant frequency for each pixel. On the output line, the signal is boosted by a cryogenic low noise amplifier, then is down-converted to the base band and acquired by an Analog to Digital Converter (ADC). Finally, the useful signal is computed on-board with an FPGA: each output tone is compared to a copy of the input tones kept as a reference, so that for each pixel we extract the in phase (I) and quadrature (Q) components of the signal.

The knowledge of the I and Q components alone does not give full access to the change in resonance frequency due to an incoming optical signal. To do so we also modulate the frequency on the local oscillator (by few kHz) synchronously to the

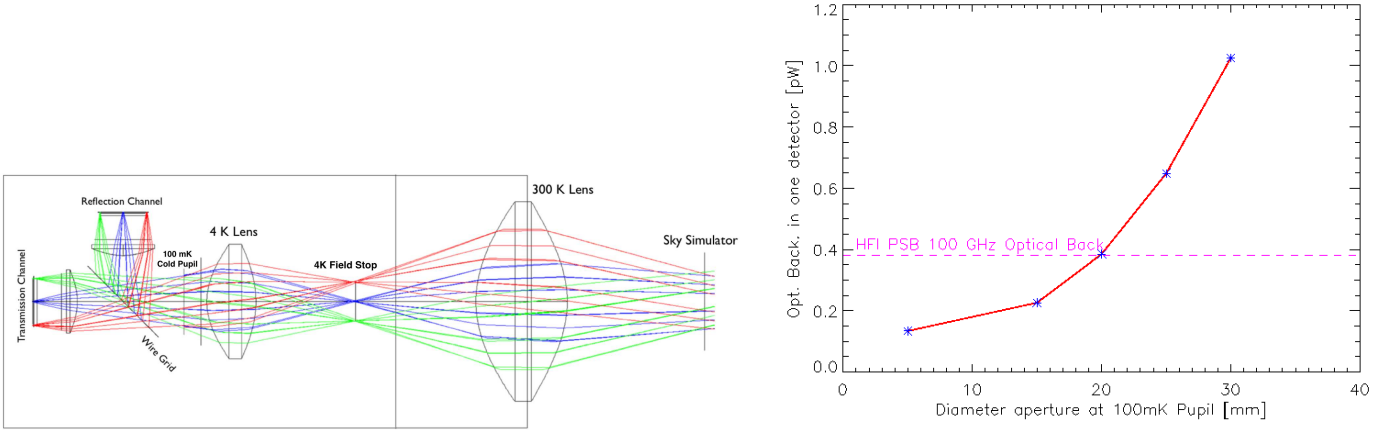


Fig. 2. Left: Ray-tracing snapshot of the cold optics inside the cryostat. Right: optical background estimation as a function of 100 mK cold stop aperture diameter (red line). We compare this results to the optical background measured in the HFI 100 GHz channel (violet dashed line).

FPGA in order to recover the differential values dI , dQ in addition to I and Q components. More details of this technique are presented in Calvo et al. (2013).

3. Optical Background Control

In order to characterise the optical response of the Ti-Al array we use a testing device called *Sky Simulator* (hereafter SS). It was originally built in order to mimic the typical ground optical background for the NIKA instrument at the IRAM 30 m telescope in Pico Veleta (Monfardini et al. 2011). The working principle is based on cooling down a black disk of 25 cm diameter by using a single-stage pulse-tube refrigerator. The SS temperature can be controlled between 50 K and 300 K. This allows us to efficiently estimate the optical detector response and the NEP. The spectral response of the detectors is derived from a classic Martin-Puplett Interferometer (hereafter MPI) based on a blackbody source modulated between 300 K and 77 K and fully polarised by a wire-grid.

The optical coupling between the SS (or the MPI) and the detectors is ensured by cold refractive optics. The optical system consists of a 300 K window lens, a field stop plus a lens at the 4 K stage. A 60 mm aperture stop and a lens are placed at the 100 mK stage in front of the back-illuminated LEKID arrays. Finally, in order to acquire data simultaneously with two independent RF channels a wire-grid polariser acts as beam splitter for the two

arrays. The left panel of Fig 2 shows a 2-D layer snapshot from a ray-tracing simulation used to optimise the optical system.

The pixel throughput⁵ is derived from the sky-simulator diameter, the fraction of un-vignetted pupil defined by the cold field stop, and the receiver pixel size with respect to diffraction pattern. We obtain:

$$A\Omega_{pixel} = (\pi/4)(u\lambda)^2$$

where u is the pixel angular size in units of $F\lambda$ (λ = wavelength and F = f-number or relative aperture), which is equal to 0.75.

The spectral band is defined by a series of low-pass metal mesh filters, placed at different cryogenic stages in order to minimise the thermal loading on the detectors. A last 3.7 cm^{-1} low pass filter is mounted in front of the LEKID array at 100 mK. The final bandpass is determined by this filter at high frequencies and by the superconducting gap cut-off at low frequencies.

We performed an optical simulation of the system accounting for the absorption, reflection and emission of the polyethylene lenses and the diffracted beam due to the cold aperture stop at 100 mK to estimate the optical background on the focal plane. The results of this simulation have been validated by comparing the optical background on NIKA Aluminium arrays for laboratory tests to the one measured at the 30 m IRAM telescope. We estimate a level of uncertainties of about 50 %. In order to re-scale the total optical background on each pixel to the typical in-flight optical background at 100 GHz, we reduced the cold aperture from 60 to 20 mm obtaining an incoming optical power of about 0.4 pW (see Fig 2).

4. Performance testing

For a complete understanding of the detectors performance and to characterise the single-pixel sensitivity, we have performed laboratory measurements during the last year. The experimental tool is optimised to work under low optical background representative of the in-space sky emission at 100 GHz. The characterisation of the optical responsivity and noise is performed using as source the SS; the spectral response is measured with the MPI. The LEKID array is cooled at a base temperature of

⁵ The throughput is the name of the optical invariant that is used for the product of the pupil area and the solid angle subtended at this pupil.

Ti-Al Film	
Valid Pixels [#]	18
Pixel size [mm]	2.3
Film Thickness [μm]	10-25
Polarised Sensitive Detectors	yes
Angular size ($F\lambda$)	0.75
Overall optical efficiency [%]	30
Total background [pW]	0.4

Table 1. Characteristics of the instrumental setup used for the measurements. The total background is calculated per pixel using a realistic optical simulation.

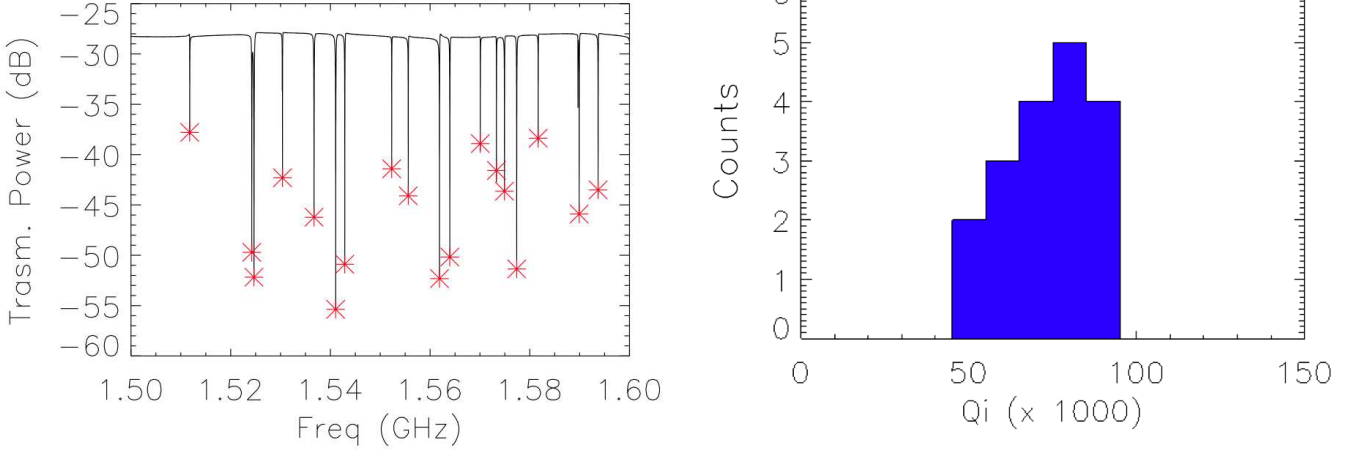


Fig. 3. Left: frequency sweep of the first generation of 25 pixels Al-Ti array. Right: internal quality factor distribution.

100 mK thanks to a closed-cycle $^3\text{He} - ^4\text{He}$ dilution cryostat designed for optical measurements. The cryostat also hosts two independent RF channels, each one equipped with a cold low-noise amplifier optimised to work at the detectors frequencies. As KIDs detectors are sensitive to the Earth magnetic fields and to those induced by the instrumentation present in the laboratory, two magnetic shields have been added to reduce this noise source: a mu-metal screen at the 300 K stage and a superconducting lead screen on the 1 K stage. We summarise in Tab 1 the main characteristics of the experimental setup.

4.1. Electrical Properties

In order to identify the LEKID resonances we performed a frequency sweep with the array connected to the VNA. The result is shown in Fig 3. We clearly see that the feed-line is not affected by the presence of standing waves supported by the slot-line modes. This is possible thanks to the bondings added between the substrate and the holder and across the feed-line. In consequence, the depth of the different resonances (i.e. the internal quality factor) is quite uniform. The pixels resonate between 1.5 and 1.6 GHz and present homogeneous internal quality factors of $8 \cdot 10^4$ (see Fig 3). Thus, each resonance occupies a bandwidth of about 20-30 kHz for an optical background of about 0.4 pW.

The critical temperature is measured with the VNA connected to the array and warming up slowly the 100 mK stage up to the superconducting transition. The transition is observed at 900 ± 25 mK in good agreement with expectations (see Sec. 2.1). Using Eq. 1, we expect a cut-off due to the superconducting gap at 65 GHz.

The normal-state sheet resistance of the Ti-Al bilayer has been measured around $R_s = 0.5$ Ohm/square at 1 K. This value is related to the measured critical temperature and the surface inductance (estimated at 1 pH/sq as expected for the thickness considered) through the relation (Leduc et al. 2010):

$$L_s = \frac{\hbar R_s}{\pi \Delta}$$

where Δ is the superconducting gap. The three electrical values (Δ , L_s and R_s), measured or estimated independently, are in agreement within 10% according to the cited relation.

4.2. Spectral Transmission

The gap of the Ti-Al bilayer has been measured from the absorption spectra taken in the lab using the MPI. The results are shown in Fig 4. We observe that below roughly 65 GHz a very low level of radiation is transmitted (less than 5 %). This means that the resultant energy gap for the Ti-Al films is $\approx 135 \mu\text{eV}$, in agreement with the critical temperature. The corresponding spectrum bandwidth⁶ $\Delta\nu/\nu$ has been measured equal to 0.28.

⁶ the bandwidth is defined as $\Delta\nu/\nu = \frac{FWHM}{\nu_0}$ where the *FWHM* is the full width at half maximum of the spectrum and ν_0 is the central frequency.

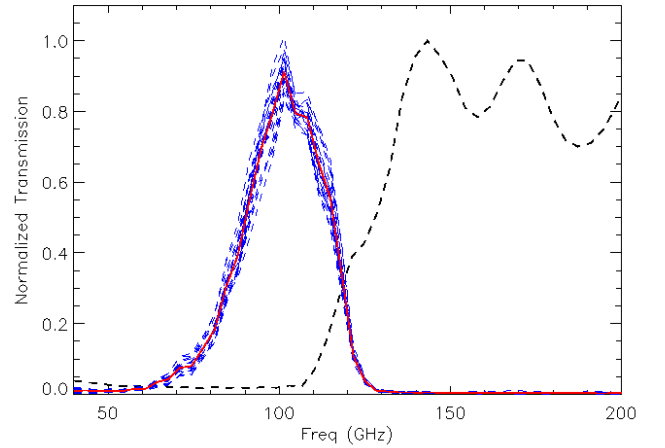


Fig. 4. Individual detector (blue dashed lines) and averaged (red line) normalised Ti-Al spectral response ($\Delta S_i / \max(\Delta S_i)$ where ΔS_i is the response of the i -th pixel). The dispersion level between pixels is of the order of few per cent. For illustration, the spectral response of the Ti-Al array is compared to the one of a pure 18 nm thick Aluminium LEKID array with a T_c of roughly 1.4 K (dashed black line).

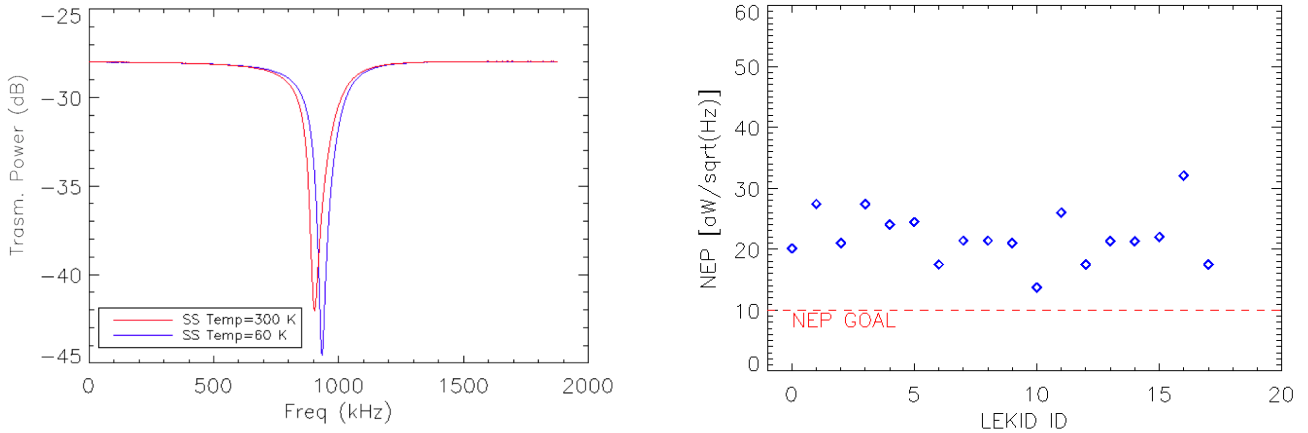


Fig. 5. Left: resonant frequency shift due to the variation of the SS temperature from 80 K to 300 K. Right: individual pixel sensitivities (blue diamonds) measured during tests compared to the reference goal (dashed red line).

4.3. Optical Response and Noise Equivalent Power

The optical responsivity of the pixels has been measured using the VNA. We perform frequency sweep to measure the LEKID transfer function for various SS background temperatures. In Fig 5 we present the shift of the resonant frequency for one pixel when the SS temperature is changed from 80 to 300 K. This frequency shift averaged across all the pixels correspond to about 27 kHz. Using the optical model we estimate the corresponding variation in optical power per pixel to about 0.3 pW. Therefore, the averaged responsivity for the array is $\mathfrak{R} = 90 \text{ kHz/pW}$.

The spectral noise density $S_n(f)$ (in $\text{Hz}/\sqrt{\text{Hz}}$), is calculated at a fixed SS temperature of 80 K using the NIKEL electronics. Correlated electronic noise is removed by subtracting a common mode. This is obtained by averaging the Time-Ordered-Data (TOD) of all detectors in the array. The resulting template is fitted linearly to the TOD of each detectors. The best-fit is then subtracted from the detectors TODs. After de-correlation, the spectral noise density is flat in a band between 1 and 10 Hz and equal to about $S_n(f) = 1 - 3 \text{ Hz}/\sqrt{\text{Hz}}$. We can easily compute the NEP as:

$$NEP = \frac{S_n(f)}{\mathfrak{R}}$$

The right panel of Fig 5 shows the NEP of individual pixels. The best pixel has a NEP equal to $1.4 \cdot 10^{-17} \text{ W/Hz}^{0.5}$. The averaged NEP over all the array is $2.2 \cdot 10^{-17} \text{ W/Hz}^{0.5}$ which is about twice the goal.

5. Conclusion

We have produced and tested high quality LEKID detectors based on multi-layers superconductors films. They have proved to be sensitive in the frequency range from 80 to 120 GHz.

- We achieved internal quality factors exceeding $5 \cdot 10^4$ under a typical space-like optical background of 0.4 pW, and we control the transition temperature as expected from calculations.
- The spectral response is in agreement with the design. It peaks at 100 GHz with a 28 % bandwidth.

- The Noise Equivalent Power is pretty uniform across the array; the best pixels approach the reference NEP goal. On average the NEP is of the order of twice the goal.

Notice that the LEKID design adopted for this study was originally developed for thin (less than 20 nm) Aluminium films, and ground-based typical optical backgrounds. The sensitivity could thus be further improved by optimising, for example, the films, back-short and substrate thicknesses, the resonator coupling to the RF feed-line and the meander geometry. Building on these promising results, larger arrays (hundreds pixels) will be developed in order to investigate and mitigate, as we did already for Aluminium films, systematic effects like for example crosstalk between pixels and homogeneity over the array.

Acknowledgements. The engineers more involved in the experimental setup development are: Gregory Garde, Henri Rodenas, Jean-Paul Leggeri, Maurice Grollier, Guillaume Bres, Christophe Vescovi, Jean-Pierre Scordilis, Eric Perbet. We acknowledge more in general the crucial contributions of the whole Cryogenics and Electronics groups at Institut Néel and LPSC. The arrays described in this paper have been produced at the CEA Saclay and PTA Grenoble microfabrication facilities. This work has been supported as part of a collaborative project, SPACEKIDS, funded via grant 313320 provided by the European Commission under Theme SPA.2012.2.2-01 of Framework Programme 7.

References

- Adam, R., Comis, B., Macías-Pérez, J. F., et al. 2014, *A&A*, 569, A66
- Bennett, C. L., Larson, D., Weiland, J. L., et al. 2013, *ApJS*, 208, 20
- Bourrion, O., Vescovi, C., Bouly, J. L., et al. 2012, in *Society of Photo-Optical Instrumentation Engineers (SPIE) Conference Series*, Vol. 8452, Society of Photo-Optical Instrumentation Engineers (SPIE) Conference Series
- Bueno, J., Coumou, P. C. J. J., Zheng, G., et al. 2014, *Applied Physics Letters*, 105, 192601
- Calvo, M., D’Addabbo, A., Monfardini, A., et al. 2014, *Journal of Low Temperature Physics*, 176, 518
- Calvo, M., Roesch, M., Désert, F. X., et al. 2013, *Astronomy and Astrophysics*, 551, L12
- Catalano, A., Calvo, M., Ponthieu, N., et al. 2014, *A&A*, 569, A9
- Cooper, L. N. 1961, *Physical Review Letters*, 6, 689
- Day, P. K., LeDuc, H. G., Mazin, B. A., Vayonakis, A., & Zmuidzinas, J. 2003, *Nature*, 425, 817
- Doyle, S. 2008, PhD Thesis, 1, 193
- Doyle, S., Naylon, J., Mauskopf, P., Porch, A., & Dunscombe, C. 2007, in *Eighteenth International Symposium on Space Terahertz Technology*, ed. A. Karпов, 170

- Doyle, S., Naylor, J., Mauskopf, P., et al. 2008, in Society of Photo-Optical Instrumentation Engineers (SPIE) Conference Series, Vol. 7020, Society of Photo-Optical Instrumentation Engineers (SPIE) Conference Series, 0
- Fauvet, L., Macías-Pérez, J. F., Aumont, J., et al. 2011, *A&A*, 526, A145
- Fauvet, L., Macías-Pérez, J. F., & Désert, F. X. 2012, *Astroparticle Physics*, 36, 57
- Hu, W. & White, M. 1997, *New A*, 2, 323
- Irwin, K. D. & Hilton, G. C. 2005, in *Cryogenic Particle Detection*, ed. C. Enss, Topics in Applied Physics No. 99 (Springer Berlin Heidelberg), 63–150
- Kogut, A., Banday, A. J., Bennett, C. L., et al. 1996, *ApJ*, 470, 653
- Kogut, A., Fixsen, D. J., Chuss, D. T., et al. 2011, *J. Cosmology Astropart. Phys.*, 7, 25
- Leduc, H. G., Bumble, B., Day, P. K., et al. 2010, *Applied Physics Letters*, 97, 102509
- Martinis, J. M., Hilton, G. C., Irwin, K. D., & Wollman, D. A. 2000, *Nuclear Instruments and Methods in Physics Research A*, 444, 23
- Matsumura, T., Akiba, Y., Borrill, J., et al. 2014, *Journal of Low Temperature Physics*, 176, 733
- Mennella, A., Bersanelli, M., Butler, R. C., et al. 2011, *A&A*, 536, A3
- Monfardini, A., Benoit, A., Bideaud, A., et al. 2011, *ApJS*, 194, 24
- Planck Collaboration, Ade, P. A. R., Aghanim, N., et al. 2014, *A&A*, 571, A16
- Planck Collaboration (2013 results I). 2014, *A&A*, in press, [arXiv:astro-ph/1303.5062]
- Planck HFI Core Team, Ade, P. A. R., Aghanim, N., et al. 2011, *A&A*, 536, A4
- Planck Collaboration, Ade, P. A. R., Aghanim, N., et al. 2014, *ArXiv e-prints*
- Swenson, L. J., Day, P. K., Eom, B. H., et al. 2013, *Journal of Applied Physics*, 113, 104501
- Usadel, K. D. 1970, *Physical Review Letters*, 25, 570
- Zmuidzinas, J. 2012, *Annual Review of Condensed Matter Physics*, 3, 169